ceramics

MDPI

Article

The Impact of BiF_3 Doping on the Yb^{3+} to Yb^{2+} Reduction during the $LiYF_4$:Yb^{3+} Crystal-Growth Process

Amir Khadiev [1], Niyaz Akhmetov [1], Stella Korableva [1], Oleg Morozov [1,2], Alexey Nizamutdinov [1,*], Vadim Semashko [1,2], Maksim Pudovkin [1] and Marat Gafurov [1,*]

[1] Institute of Physics, Kazan Federal University, Kremlevskaya, 18, 420008 Kazan, Russia
[2] Zavoisky Physical-Technical Institute, FRC Kazan Scientific Center of RAS, Sibirskii Ave., 10/7, 420029 Kazan, Russia
* Correspondence: anizamutdinov@mail.ru (A.N.); mgafurov@gmail.com (M.G.)

Abstract: Here, we report on the opportunity to suppress Yb^{3+} to Yb^{2+} dopant-ion reduction in $LiYb_xY_{1-x}F_4$ mixed crystals during growth processes, using the Bridgmen–Stocbarger technique in graphite crucibles in vacuum. This was carried out by the additional doping of the LiF-YF_3-YbF_3 powder mixture with 1% of BiF_3 additive. The crystals of $LiY_{0.8}Yb_{0.2}F_4$ and $LiY_{0.8}Yb_{0.2}F_4$ with BiF_3 doping in the charge, were grown. The spatial distribution of the spectral-kinetic properties of Yb^{3+} and Yb^{2+} ions along the grown crystalline-boules were studied. It was established that the Yb^{2+} concentration rises during the $LiY_{0.8}Yb_{0.2}F_4$ crystal-growth processes without the BiF_3 additive: the absorption coefficient of Yb^{2+} (π-polarization) at 340 nm rises from 0 (at the beginning of the boule) to 2.5 cm^{-1} (at the end of the boule). In contrast, the undetectable absorption of Yb^{2+} along the crystals grown from the BiF_3 doped melt was displayed. The luminescence-decay time of Yb^{3+} decreases from 3.7 to 1.8 ms from the beginning to the end of the $LiY_{0.8}Yb_{0.2}F_4$ boule grown from the BiF_3 undoped melt, and stays constant (~3.7 ms) along the samples grown with BiF_3. Here we demonstrate a positive effect of BiF_3 doping on the optical homogeneity of $LiYF_4$:Yb^{3+} crystals.

Keywords: fluoride crystals; impurity ion-distribution; impurity ion redox-processes; rare-earth ions; Yb^{2+} and Yb^{3+} ions spectroscopy

check for updates

Citation: Khadiev, A.; Akhmetov, N.; Korableva, S.; Morozov, O.; Nizamutdinov, A.; Semashko, V.; Pudovkin, M.; Gafurov, M. The Impact of BiF_3 Doping on the Yb^{3+} to Yb^{2+} Reduction during the $LiYF_4$:Yb^{3+} Crystal-Growth Process. *Ceramics* **2022**, *5*, 1198–1206. https://doi.org/10.3390/ceramics5040085

Academic Editor: Francesco Scotognella

Received: 31 October 2022
Accepted: 28 November 2022
Published: 6 December 2022

1. Introduction

$LiYF_4$ fluoride crystals doped with Yb^{3+} ions are well-known continuous-wave laser materials with room temperature tuning-ranges of 997–1065 nm and 998–1076 nm for σ and π polarizations, respectively [1]. Due to the large gain-bandwidth, the $LiYF_4$:Yb^{3+} crystals can be implemented as an active medium to obtain laser oscillation in a subpicosecond-pulse regime under cryogenic cooling [2]. The unique energy-level structure of Yb^{3+} ions determines the high efficiency of the optical-refrigeration effect. For example, an active medium based on $LiYF_4$:Yb^{3+} can reduce the temperature the of GaAs/InGaAs double-heterostructure with 2 µm thickness, down to 165 K [3].

Common problems which reduce efficiency for both laser performance [4–6] and laser cooling [7] is the conversion of Yb ions from a trivalent to a divalent state. Ions such as Sm^{3+} and Eu^{3+} also demonstrate the same tendency. The optical properties of Yb^{2+} ions were investigated in oxides [8], various fluorides [9,10], and fibers [5]. Due to the completed 4f electron shell of Yb^{2+}, its absorption spectrum is formed by interconfigurational 4fn→4fn-1 5d transitions, corresponding to the 170–400 nm spectral range [11]. In addition, the intervalence charge transfer can be observed in Yb^{3+}-Yb^{2+} mixed systems [12], which may affect the luminescent properties of Yb^{3+}.

Part of the Yb^{3+} ions distributed in the host-matrix can be reduced to divalent state under specific crystal-growth conditions [13]. In the work [14], the authors identify some of these conditions, namely: (a) an absence of oxidizer, (b) the trivalent rare-earth ion

must substitute the cation with the different valence, (c) a proximity of ionic radii of the trivalent activator and the divalent host-cation, and (d) an appropriate host-compound conducive to dopant valence-reduction. Generally, the $LiYF_4$ host-matrix does not satisfy any of these conditions and does not have sites for the divalent dopant; therefore, the divalent-ytterbium appearance should be associated with impurities or defects. However, the most urgent problem for the optically perfect fluoride-crystal-growth process is the presence of incontrollable oxides and the OH^- group containing impurities in the charge. Indeed, the water traces always exist in the growth-chamber environment [15].

A common way to deal with Yb^{3+}-Yb^{2+} conversion is the conduction of crystal-growth procedures under a fluorinating atmosphere, for example, in the presence of HF or CF_4 gases [16]. As mentioned above, despite the effectiveness of this method, the use of a fluorinating atmosphere is related to notable technical difficulties. It is worth keeping in mind the fact that the additional Bi-doping procedure can improve the optical properties of rare-earth-doped aluminosilicate, borate, phosphate and germanate glasses [17]. This occurs due to the high electron-affinity of Bi^{3+} ions and the consequent effective reduction into a lower valence-state [18]. In addition, it is known that the Yb^{3+} and Bi^{+} ions being doped to the matrix as a pair mutually stabilizes their valence, which was shown in the PbF_2 matrix, where the conditions are in favor of Yb^{2+} ions formation [19]. In this study, we demonstrate the fact that the addition of BiF_3 to the LiF-YF_3-YbF_3 charge reduces the divalent-ytterbium-formation efficiency in $LiYF_4$:Yb^{3+}-solid solutions grown by Bridgeman technique in graphite crucibles in vacuum.

2. Materials and Methods

2.1. Material Synthesis

The crystals of $LiY_{0.8}Yb_{0.2}F_4$ were grown in graphite crucibles from the melt with and without 1% of BiF_3 additive, using the Bridgman technique. The fluorides of the Yttrium, Ytterbium and Bismuth powder-mixture was used as the charge. During the growth procedure, the pressure inside the crystal-growth chamber was maintained at 10^{-4} mbar. The melt was pulled out from the high temperature zone through a region of a thermal gradient (≈100 °C/cm). To obtain the specific optical *c*-axis-orientation (perpendicular to the cylinder of the boule), a seeding crystal was placed inside the crucible.

Samples were cut into a parallelepipeds with 5 × 5 × 30 mm typical dimensions. The optical axis of the crystals was perpendicular to one of the carefully polished facets.

2.2. Spectral-Kinetic Characterization of the Samples

The absorption spectra of the samples were obtained via the one-beam method, using StellarNet SL5 Deuterium/Halogen Light Source (spectral range 190–2500 nm, StellarNet, Inc. 14390 Carlson Circle Tampa, FL, USA). The experimental set-up is presented in Figure 1.

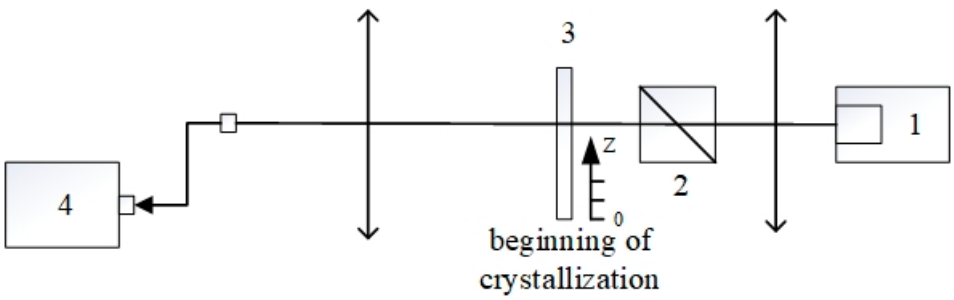

Figure 1. The experimental setup for registration of the absorption spectrum of the samples. (1) broad-band StellarNet halogen and deuterium light-source; (2) Glan–Taylor prism; (3) the sample; (4) CCD StellarNet spectrometer. The samples were moved along the *z*-axis that is perpendicular to the probe beam.

A Glan prism was used as the polarizer. Incident light (the probe beam) was focused on the sample surface using a fused-silica lens with a 5 cm focal length. Luminescence and absorption spectra were registered using the StellarNet CCD spectrometer (optical resolution up to 0.5 nm, StellarNet, Inc. 14390 Carlson Circle Tampa, FL, USA). The relative accuracy of the light-intensity measurements was approximately 0.5%. Luminescence excitation was carried out using pulse-periodic radiation of the InAlGaAs laser diode ATC-C1000-100 (FWHM 3 nm, "Semiconductor devices" LLC, Moscow, Russia) operating at 935 nm wavelength. Excitation laser-pulse duration and pulse repetition rate were 5 ms and 10 Hz, respectively. Luminescence-decay curves were detected using the monochromator DMR-4 (OPTICS LLS, Moscow, Russia), the photomultiplier FEU-62 (ZAPADPRIBOR LLC, Moscow, Russia, 400–1200 nm operating spectral range), and the Bordo 211 digital oscillograph (AURIS LLC, Moscow, 10 bit and 200 MHz bandwidth).

3. Results and Discussion

Absorption and Luminescence Spectrum of $LiY_{0.8}Yb_{0.2}F_4$ and $LiY_{0.8}Yb_{0.2}F_4$:BiF_3 (1%)

Spin-orbit interaction splits the ^2F term of the Yb^{3+} ion into two $^2F_{5/2}$ and $^2F_{7/2}$ manifolds, where $^2F_{7/2}$ is the ground state. These manifolds split into three and four Stark sub-levels, respectively. The polarized absorption spectra of the crystals are shown in Figure 2.

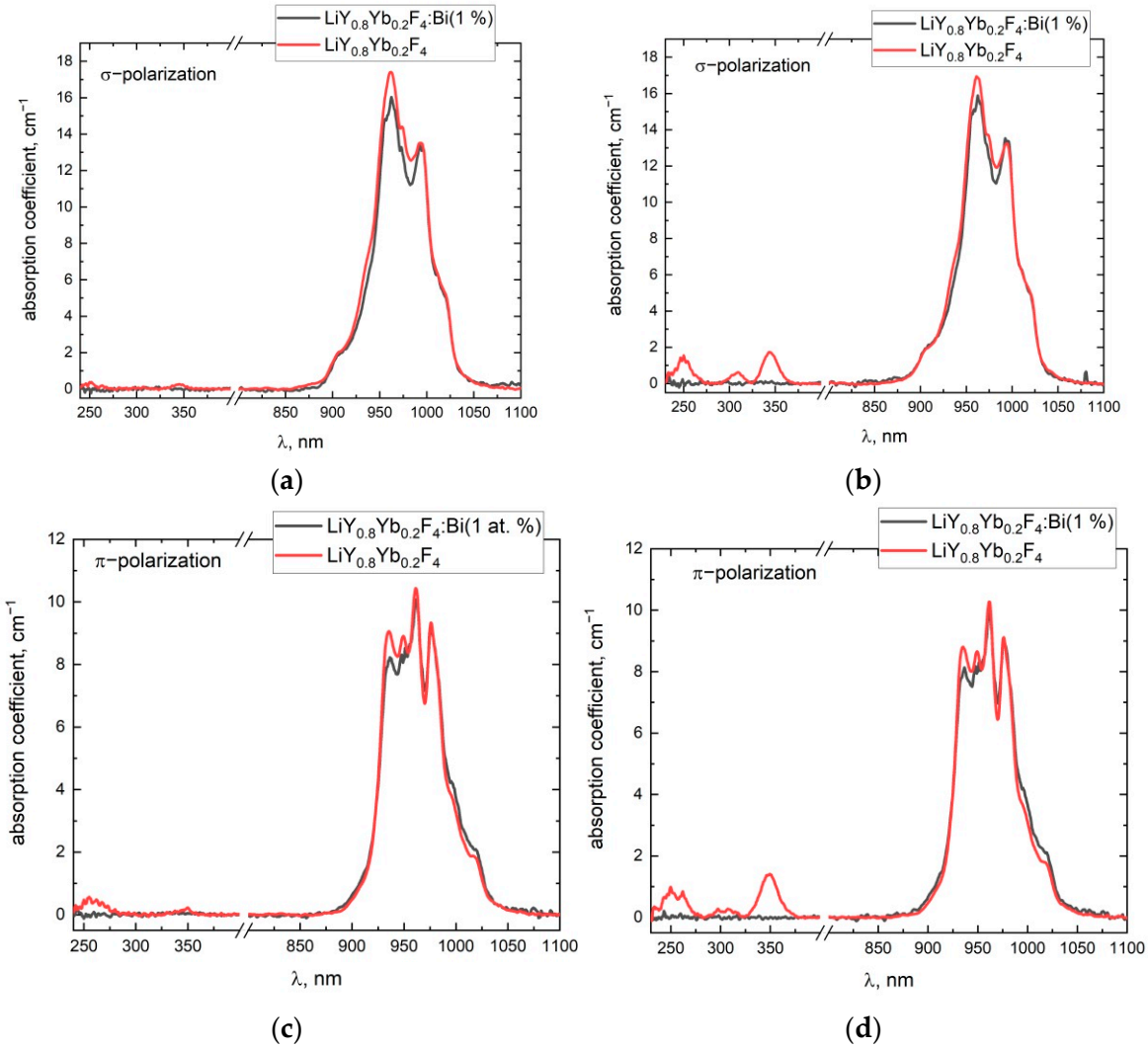

Figure 2. Polarized absorption spectra of two different parts of the $LiY_{0.8}Yb_{0.2}F_4$ and $LiY_{0.8}Yb_{0.2}F_4$:BiF_3 (1%) crystals (**a**,**c**)—the beginning of crystallization, (**b**,**d**)—the end of crystallization.

Each infra-red spectrum represents six absorption bands, due to the selection rules for each polarization [20]. These results are in agreement with an already published paper [21]. Four absorption peaks in the ultraviolet spectral-range can be distinguished at 248 nm, 262 nm, 307 nm, and 347 nm. These absorption bands are also in good agreement with the M. Kaczmarek et al. paper [22], in which the Yb^{2+} impurity centers in $LiYF_4$ crystals were induced by X-ray radiation. In our study, Yb^{2+} centers can appear in $LiYF_4$:Yb^{3+} crystals during the growth process because the vacuum and the contact of the melt with the graphite crucible are the reducing conditions. In addition, the absorption spectra change significantly in different parts of the crystal boule. It can be seen from Figure 2, that the absorption bands in the UV range are more intense for the part corresponding to the end of the crystallization process, whereas the bands are almost not pronounced at the beginning of crystallization. The nonpolarized normalized-luminescence-spectra of the $LiY_{0.8}Yb_{0.2}$ and $LiY_{0.8}Yb_{0.2}$ with BiF_3 additives (1 at. % in the charge) samples under 934 nm laser-excitation, are represented in Figure 3.

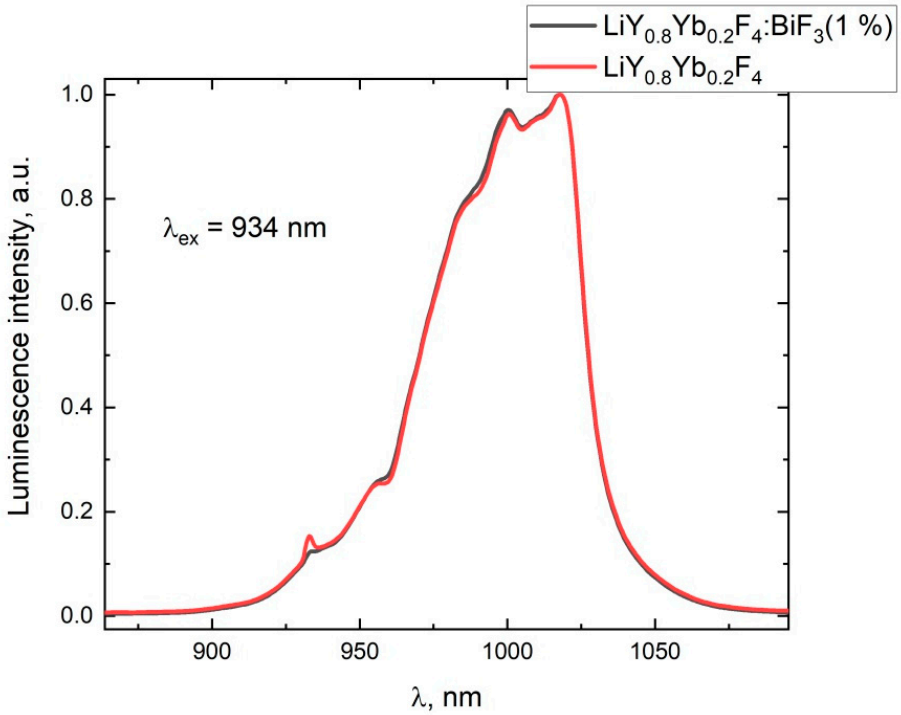

Figure 3. The normalized luminescence-spectra of the $LiY_{0.8}Yb_{0.2}$ and $LiY_{0.8}Yb_{0.2}$:BiF_3 (1%) samples under 934 nm laser-excitation.

The BiF_3 additive does not change the luminescence spectra of the Yb^{3+} ions in the samples, but affects the fluorescence-kinetic properties. The drastic shortening of the luminescence-decay time of the Yb^{3+} ions along the crystalline boule (with growth time) is observed for the samples without the BiF_3 additive in the charge (Figure 4). In contrast, the Yb^{3+} life-time was constant for any part of the sample grown from the BiF_3-doped charge.

Due to the simultaneous increase in absorption in the ultraviolet spectral-range and the shortening of the Yb^{3+} luminescence-decay time, it can be assumed that there are energy-transfer processes between Yb^{2+} and Yb^{3+} ions in $LiYF_4$:Yb^{3+} single crystals. This can be associated with the well-known fact that Yb^{3+} and Yb^{2+} ions can form complex charge-transfer states [23]. The origin and the real mechanism of the interaction require further investigation.

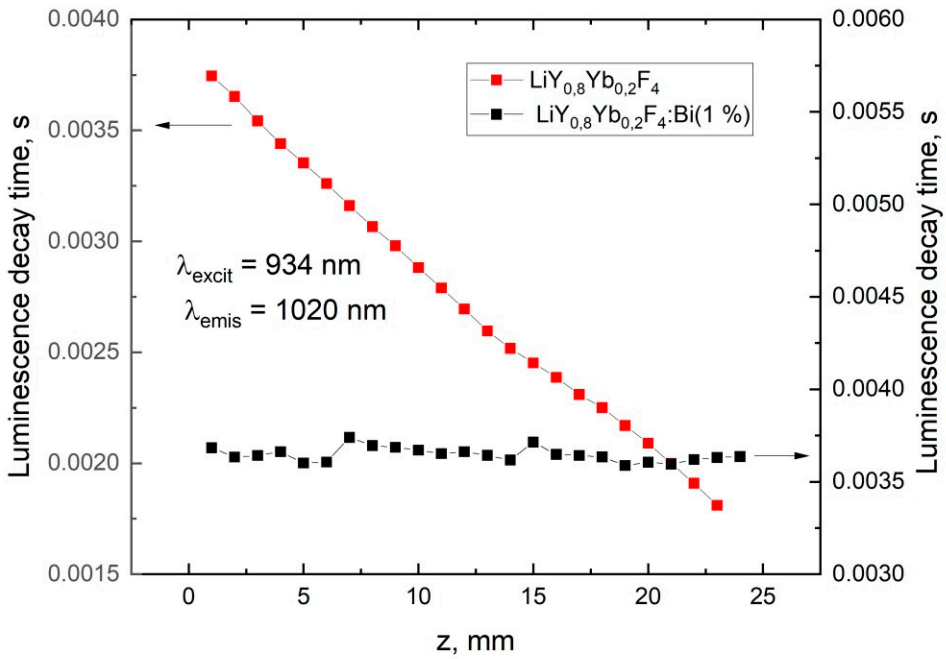

Figure 4. Luminescence-decay time of Yb^{3+} (1020 nm) under 934 nm excitation along the crystals (along *z*-axis).

It is important to note that the presence of Bi ions in the samples does not manifest itself in the optical spectra. There are two reasons for this: (1) the bismuth in any valence state is absent or the concentration is too low in the samples, due to the volatility of the Bi-components; (2) the Bi has a valence state in the grown crystal which cannot be detected in the visible and near-IR spectral-ranges. That is why we have studied the impact of the BiF_3 doping effect on the spectroscopic properties of Yb^{3+} and Yb^{2+} ions along the crystalline boule.

The dopant concentration is proportional to the absorption coefficient, and their distribution can be described by the Gulliver–Pfann law [24]:

$$C(g(z)) = C_0 * k_{eff} * (1 - g(z))^{k_{eff}-1}, \quad (1)$$

where k_{eff} is the effective dopant-segregation coefficient, $g(z)$ identifies the specific part of the crystal which can be expressed as: $g(z) = z/L$, where L is the total length of the sample and z is the distance from the beginning of crystallization.

Figure 5 shows the dependencies of the polarized absorption-coefficient at 340 nm of the $LiY_{0.8}Yb_{0.2}F_4$ crystal samples grown from the melt, with and without 1%of BiF_3 additive along the direction of growth, where z = 0 corresponds to the beginning of sample crystallization. The sample of crystal grown from the BiF_3-doped melt demonstrates no detectable absorption in the ultraviolet spectral-range at any part of the crystal boule.

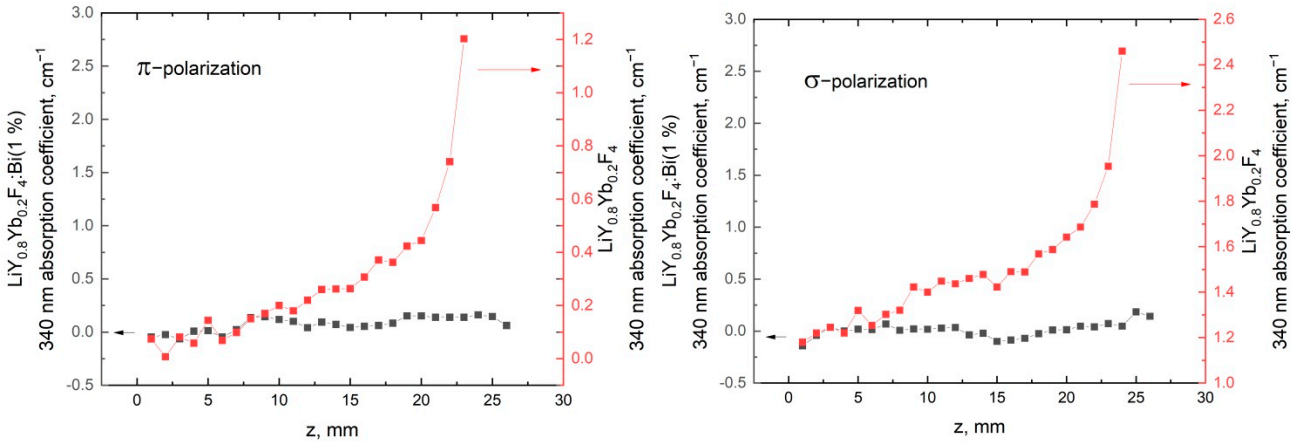

(**a**) (**b**)

Figure 5. Absorption coefficient at 340 nm along the$LiY_{0.8}Yb_{0.2}F_4$ crystals grown from the melt, with and without 1% of BiF_3 additive for π (**a**) and σ (**b**) polarizations.

The distribution coefficient of Yb^{3+} ions in the $LiYF_4$ crystals should be close to 0.96, due to the isomorphic substitution of Y^{3+} by the Yb^{3+} ions [25]. In our $LiY_{0.8}Yb_{0.2}F_4$ sample, we observed the decrease in Yb^{3+} concentration with a simultaneous increase in ultraviolet absorption (Figure 6) along the boule, from the beginning of crystallization to the end.

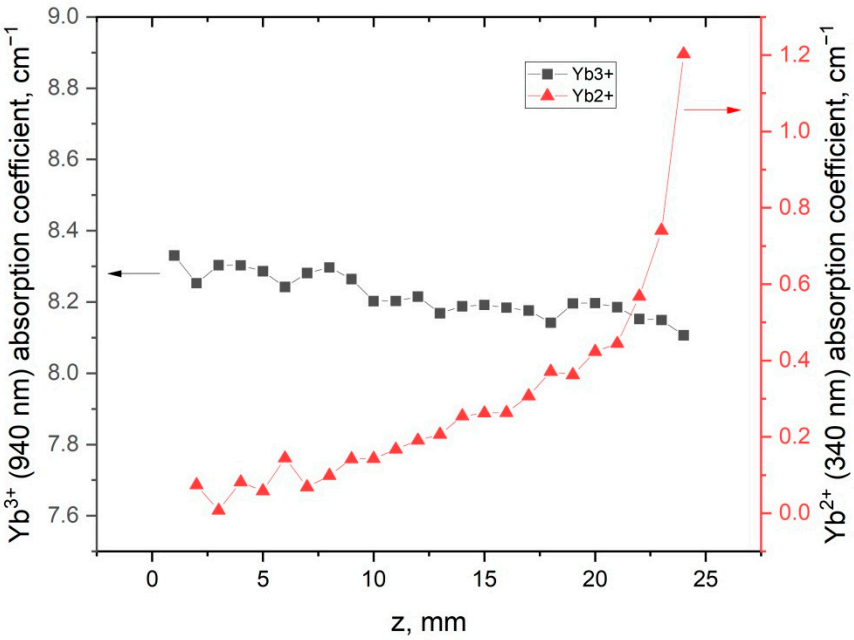

Figure 6. Yb^{3+} and Yb^{2+} absorption-coefficient along the $LiY_{0.8}Yb_{0.2}F_4$ crystal.

This relation between trivalent- and divalent-ytterbium absorption-coefficients is the indirect evidence of reduction processes occurring during crystal growth. Several studies devoted to the investigation of Yb^{2+} distribution along fluoride crystals found that the segregation coefficient of Yb^{2+} in YbF_3:CaF_2 crystals varies from 0.68 to 0.74, depending on Yb concentration [26]. In YbF_3:BaF_2, the segregation coefficient of divalent ytterbium equals 0.59 [24]. The implementation of formula (1) on the dependencies in Figure 6 gives the effective-distribution-coefficient values 0.98 and −0.7 for Yb^{3+} and Yb^{2+}, respectively. Because k_{eff} must be positive, the Yb^{2+} ion content distribution along the crystal boule cannot be described by the Gulliver–Pfann equation. It can probably be explained by the high volatility of the bismuth salts and $LiBiF_4$ compound. It means that the chemical

composition of the melt and the crystallization conditions are drastically changed with the time of the crystal-growth process, which contradicts the basic assumptions in the derivation of the Galiver–Pfann law.

In addition, it has to be taken into account that, besides the significant rise in ultraviolet absorption, there is a drastic shortening of the luminescence-decay time of the Yb^{3+} ions along the crystal without Bi doping, which is not evident for the $LiY_{0.8}Yb_{0.2}F_4$:BiF_3 (1%) sample (Figure 7).

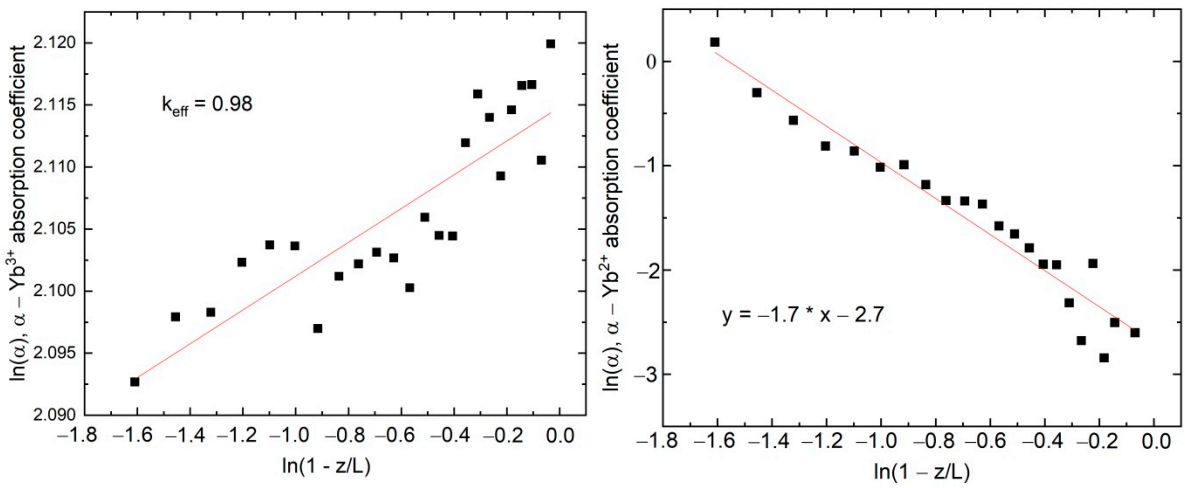

(**a**) (**b**)

Figure 7. (**a**) Yb^{3+} and (**b**) Yb^{2+} absorption along the $LiY_{0.8}Yb_{0.2}F_4$ crystal in ln(α) vs. ln(1−z/L) coordinates, where α is the absorption coefficient, z represents the beginning of the sample crystallization, and L is the full length of the sample.

The origin and the exact mechanism of the interaction require further investigation. It is known that Yb^{3+} and Yb^{2+} ions can form complex charge-transfer states [23]. It can be assumed that the BiF_3 additive sufficiently improves the optical quality of the $LiYF_4$:Yb^{3+} materials, which were grown using the Bridgman technique in above-mentioned conditions. Finally, it was observed, that the addition of the BiF_3 additive to the charge sufficiently improves the optical quality of the $LiYF_4$:Yb^{3+} materials, which were grown using the Bridgman technique in above-mentioned conditions.

It is also important to note that Bi doping cannot be the universal solution for the Yb^{3+}-Yb^{2+} conversion problem, due to the near-infrared absorption of the low-valence Bi ions, therefore disturbing the original spectrum of the samples. In addition, the crystallization temperature must be higher than the volatilization temperature of the BiF_3. This fact imposes some limitations on the crystals.

4. Conclusions

For the first time, the distribution of Yb^{2+} ions in $LiYF_4$:Yb^{3+} crystals was investigated. It was suggested that the formation of Yb^{2+} ions in the crystals occurs due to the growth conditions (for example, the presence of a trace quantity of water and/or synthesis in vacuum and graphite crucibles and heaters). The relation between Yb^{2+} concentration and luminescence-decay time of Yb^{3+} ions appeared to be clear and consistent. In particular, a significant increase in the Yb^{2+} absorption coefficient occurs simultaneously with Yb^{3+} luminescence quenching. The addition of BiF_3 to the melt led to the absence of the UV absorption bands corresponding to the Yb^{2+} ions. In its turn, Yb^{3+} luminescence-decay time remains stable for different parts of the crystals. The mechanism of energy transfer between Yb^{2+} and Yb^{3+} ions in heavily doped $LiYF_4$ crystals needs further investigation, because it can lower the effectiveness of the up-conversion excitation in co-doped $LiYF_4$:Yb:Tm/Ho/Eu laser crystals.

A positive effect of BiF_3 doping of the melt on the optical homogeneity of $LiYF_4$:Yb^{3+} crystals has at least been detected.

We believe that one of the main advantages of the present work is that the work reveals some useful details concerning the BiF_3-based $LiYF_4$:Yb^{3+} crystal growth. Indeed, the use of BiF_3 during the crystal-growth process seems to be beneficial compared to the alternative ways, such as the use of aggressive and toxic fluorinated-gases. In particular, in order to reduce the concentration of Yb^{2+} in the iYF_4:Yb^{3+} crystal, it is enough to add 17 mg of BiF_3 to the starting material to obtain 1 kg of $LiYF_4$:Yb^{3+} crystals. In its turn, BiF_3 powder is relatively cheap, compared to fluorinated gases. The addition of BiF_3 powder allows the exclusion of several steps in the technology of the crystal-growth process. In particular, it allows for reducing the time of the drying of the starting material from a range of 12 to 20 h, to 2 to 4 h. In addition, the use of BiF_3 allows for the performance of the preparatory pumping of the vacuum chamber up to 10^{-1}–10^{-2} Pa, compared to 10^{-4}–10^{-5} Pa (without BiF_3). It reduces the time of crystal growth or lowers the requirements imposed on the vacuum-pump system.

Author Contributions: Conceptualization, A.K., S.K., O.M., A.N., V.S. and A.K.; formal analysis, M.P., M.G. and A.N.; investigation, A.K., N.A., S.K., O.M., A.N., V.S. and A.K.; resources, M.P., M.G. and A.N.; writing—original draft preparation, A.N., A.K.; writing—review and editing, A.N., V.S., M.P. All authors have read and agreed to the published version of the manuscript.

Funding: The work was funded by the subsidy allocated to Kazan Federal University for the state assignment in the sphere of scientific activities (project number FZSM-2022-0021).

Data Availability Statement: Not applicable.

Conflicts of Interest: The authors declare no conflict of interest.

References

1. Alderighi, D.; Pirri, A.; Toci, G.; Vannini, M. Tunability enhancement of Yb:YLF based laser. *Opt. Express* **2010**, *18*, 2236–2241. [CrossRef] [PubMed]
2. Kawanaka, J.; Yamakawa, K. 30-mJ, diode-pumped, chirped-pulse Yb:YLF regenerative amplifier. *Opt. Lett.* **2003**, *28*, 2121–2123. [CrossRef] [PubMed]
3. Seletskiy, D.V.; Melgaard, S.D.; Epstein, R.I.; Di Lieto, A.; Tonelli, M.; Sheik-Bahae, M. Local laser cooling of Yb:YLF to 110 K. *Opt. Express* **2011**, *19*, 18229–18236. [CrossRef] [PubMed]
4. Kirchhof, J.; Unger, S.; Schwuchow, A.; Jetschke, S.; Reichel, V.; Leich, M.; Scheffel, A. The influence of Yb2+ ions on optical properties and power stability of ytterbium-doped laser fibers. *Opt. Compon. Mater. VII* **2010**, *7598*, 75980B.
5. Rydberg, S.; Engholm, M. Experimental evidence for the formation of divalent ytterbium in the photodarkening process of Yb-doped fiber lasers. *Opt. Express* **2013**, *21*, 6681–6688. [CrossRef]
6. Gebavi, H.; Milanese, D.; Taccheo, S.; Mechin, D.; Monteville, A.; Freyria, F.S.; Bonelli, B.; Robin, T. Photodarkening of Infrared Irradiated Yb^{3+}-Doped Alumino-Silicate Glasses: Effect on UV Absorption Bands and Fluorescence Spectra. *Fibers* **2013**, *1*, 101–109. [CrossRef]
7. Knall, J.; Vigneron, P.-B.; Engholm, M.; Dragic, P.D.; Yu, N.; Ballato, J.; Bernier, M.; Digonnet, M.J.F. Laser cooling in a silica optical fiber at atmospheric pressure. *Opt. Lett.* **2020**, *45*, 1092–1095. [CrossRef]
8. Solomonov, V.I.; Osipov, V.V.; Spirina, A.V. Luminescence and absorption of divalent ytterbium ion in yttrium-aluminum garnet ceramics. *Opt. Spectrosc.* **2014**, *117*, 441–446. [CrossRef]
9. Moine, B.; Courtois, B.; Pedrini, C. Luminescence and photoionization processes of Yb^{2+} in CaF_2, SrF_2 and BaF_2. *J. Phys.* **1989**, *50*, 2105–2119. [CrossRef]
10. Kück, S.; Henke, M.; Rademaker, K. Crystal growth and spectroscopic investigation of Yb^{2+}-doped fluoride crystals. *Laser Phys.* **2001**, *11*, 116–119.
11. Loh, E. ^4f_n-$^4f_{n-1}$5d Spectra of rare-earth ions in crystals. *Phys. Rev.* **1968**, *175*, 533–536. [CrossRef]
12. Barandiarán, Z.; Seijo, L. Intervalence charge transfer luminescence: Interplay between anomalous and 5d–4f emissions in Yb-doped fluorite-type crystals. *J. Chem. Phys.* **2014**, *141*, 23. [CrossRef] [PubMed]
13. Nicoara, I.; Stef, M.; Pruna, A. Growth of YbF3-doped CaF2 crystals and characterization of Yb^{3+}/Yb^{2+} conversion. *J. Cryst. Growth* **2008**, *310*, 1470–1475. [CrossRef]
14. Pei, Z.; Su, Q.; Zhang, J. The valence change from RE^{3+} to RE^{2+} (RE = Eu, Sm, Yb) in SrB407: RE prepared in air and the spectral properties of RE^{2+}. *J. Alloys Compd.* **1993**, *198*, 51–53. [CrossRef]
15. Baldochi, S.L.; Shimamura, K.; Nakano, K.; Mujilatu, N.; Fukuda, T. Ce-doped $LiYF_4$ growth under CF_4 atmosphere. *J. Cryst. Growth* **1999**, *205*, 537–542. [CrossRef]

16. Bensalah, A.; Shimamura, K.; Sudesh, V.; Sato, H.; Ito, K.; Fukuda, T. Growth of Tm, Ho-codoped $YLiF_4$ and $LuLiF_4$ single crystals for eye- safe lasers. *J. Cryst. Growth* **2001**, *223*, 539–544. [CrossRef]
17. Dai, N.; Xu, B.; Jiang, Z.; Peng, J.; Li, H.; Luan, H.; Yang, L.; Li, J. Effect of Yb^{3+} concentration on the broadband emission intensity and peak wavelength shift in Yb/Bi ions co-doped silica-based glasses. *Opt. Express.* **2010**, *18*, 18642–18648. [CrossRef]
18. Truong, V.G.; Bigot, L.; Lerouge, A.; Douay, M.; Razdobreev, I. Study of thermal stability and luminescence quenching properties of bismuth-doped silicate glasses for fiber laser applications. *Appl. Phys. Lett.* **2008**, *92*, 90–93. [CrossRef]
19. Zhang, P.; Chen, N.; Wang, R.; Huang, X.; Zhu, S.; Li, Z.; Yin, H.; Chen, Z. Charge compensation effects of Yb^{3+} on the Bi^{+}: Near-infrared emission in PbF_2 crystal. *Opt. Lett.* **2018**, *43*, 2372–2375. [CrossRef]
20. Sugiyama, A.; Katsurayama, M.; Anzai, Y.; Tsuboi, T. Spectroscopic properties of Yb doped YLF grown by a vertical Bridgman method. *J. Alloys Compd.* **2006**, *408*, 780–783. [CrossRef]
21. Coluccelli, N.; Galzerano, G.; Bonelli, L.; Toncelli, A.; Di Lieto, A.; Tonelli, M.; Laporta, P. Room-temperature diode-pumped Yb^{3+}-doped $LiYF_4$ and KYF_4 lasers. *Appl. Phys. B Lasers Opt.* **2008**, *92*, 519–523. [CrossRef]
22. Kaczmarek, S.M.; Bensalah, A.; Boulon, G. γ-Ray induced color centers in pure and Yb doped $LiYF_4$ and $LiLuF_4$ single crystals. *Opt. Mater.* **2006**, *28*, 123–128. [CrossRef]
23. MacKeen, C.; Bridges, F.; Kozina, M.; Mehta, A.; Reid, M.F.; Wells, J.-P.R.; Barandiarán, Z. Evidence that the anomalous emission from CaF_2:Yb^{2+} is not described by the impurity trapped exciton model. *J. Phys. Chem. Lett.* **2017**, *8*, 3313–3316. [CrossRef] [PubMed]
24. Nicoara, I.; Buse, G.; Bunoiu, M. Segregation coefficient of Yb^{3+} and Yb^{2+} ions in YbF_3 doped BaF_2 crystals. *AIP Conf. Proc.* **2014**, *1634*, 111–114.
25. Bensalah, A.; Guyot, Y.; Ito, M.; Brenier, A.; Sato, H.; Fukuda, T.; Boulon, G. Growth of Yb^{3+}-doped $YLiF_4$ laser crystal by the Czochralski method. Attempt of Yb3+ energy level assignment and estimation of the laser potentiality. *Opt. Mater.* **2004**, *26*, 375–383. [CrossRef]
26. Nicoara, I.; Pecingina-Garjoaba, N.; Bunoiu, O. Concentration distribution of Yb^{2+} and Yb^{3+} ions in YbF_3:CaF_2 crystals. *J. Cryst. Growth.* **2008**, *310*, 1476–1481. [CrossRef]